

Phase Change-Mediated Capture of Carbon Dioxide from Air with a Molecular Triamine Network Solid

Adrian J. Huang, Ankur K. Gupta, Henry Z. H. Jiang, Hao Zhuang, Malia B. Wenny, Ryan A. Klein, Hyunchul Kwon, Katie R. Meihaus, Hiroyasu Furukawa, Craig M. Brown, Jeffrey A. Reimer, Wibe A. de Jong, and Jeffrey R. Long*



Cite This: *J. Am. Chem. Soc.* 2025, 147, 10519–10529



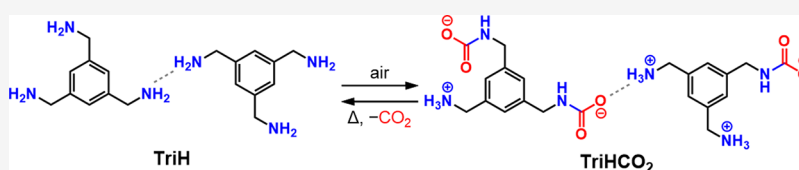
Read Online

ACCESS |

Metrics & More

Article Recommendations

Supporting Information



ABSTRACT: The efficient removal of CO₂ from exhaust streams and even directly from air is necessary to forestall climate change, lending urgency to the search for new materials that can rapidly capture CO₂ at high capacity. The recent discovery that diamine-appended metal–organic frameworks can exhibit cooperative CO₂ uptake via the formation of ammonium carbamate chains begs the question of whether simple organic polyamine molecules could be designed to achieve a similar switch-like behavior with even higher separation capacities. Here, we present a solid molecular triamine, 1,3,5-tris(aminomethyl)benzene (TriH), that rapidly captures large quantities of CO₂ upon exposure to humid air to form the porous, crystalline, ammonium carbamate network solid TriH(CO₂)_{1.5}·xH₂O (TriHCO₂). The phase transition behavior of TriH converting to TriHCO₂ was studied through powder and single-crystal X-ray diffraction analysis, and additional spectroscopic techniques further verified the formation of ammonium carbamate species upon exposing TriH to humid air. Detailed breakthrough analyses conducted under varying temperatures, relative humidities, and flow rates reveal record CO₂ adsorption capacities as high as 8.9 mmol/g. Computational analyses reveal an activation barrier associated with TriH absorbing CO₂ under dry conditions that is lowered under humid conditions through hydrogen bonding with a water molecule in the transition state associated with N–C bond formation. These results highlight the prospect of tunable molecular polyamines as a new class of candidate absorbents for high-capacity CO₂ capture.

INTRODUCTION

Direct air capture (DAC) of CO₂ is recognized as a crucial mitigation strategy to offset CO₂ emissions from hard-to-abate industries and address legacy emissions.^{1–7} When implemented alongside other mitigation strategies, DAC could help forestall the most dire effects of anthropogenic climate change.^{1,8–11} In order to meet this need, DAC must be deployed for the removal of billions of tons of CO₂ annually,^{12,13} and because of the ultradilute concentration of CO₂ in air (~420 ppm), the materials utilized in the process must exhibit high gravimetric CO₂ uptakes, rapid sorption kinetics, and stability to humid, oxygen-rich streams.^{2,14,15}

Basic aqueous solutions¹⁵ and amorphous amine-functionalized solids^{16,17} demonstrate the ability to chemisorb CO₂ selectively from air with modest capacities (generally less than 0.7 mmol/g in the latter case). Indeed, some of the related materials are employed for several small-scale DAC operations around the world.^{7,18,19} However, tremendous thermal energy is necessary to heat these materials to desorb CO₂, on the order of ~4 GJ/tCO₂ or higher,⁷ much of which is utilized as sensible heat (energy required to heat the sorbent from a lower absorption temperature to higher desorption temperature) to

release minimal quantities of CO₂ given the low CO₂ capacities of current technologies.²⁰ One potential strategy to reduce the energy consumption associated with DAC is to design new materials exhibiting significantly higher CO₂ sorption capacities by increasing the amine-site density in such materials. Operationally, materials demonstrating higher gravimetric CO₂ capacities and similar regeneration energies would reduce sensible heat energy costs when normalized to the quantity of CO₂ that is captured. As such, alongside complementary process engineering improvements, there is an urgent need for the fundamental discovery of candidate DAC materials that can capture large quantities of CO₂ at the dilute concentrations present in air.¹²

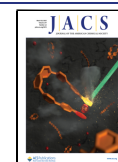
Recently, molecular amines and iminoguanidines have been demonstrated to, when dissolved in water, capture CO₂ from

Received: December 28, 2024

Revised: March 4, 2025

Accepted: March 5, 2025

Published: March 12, 2025



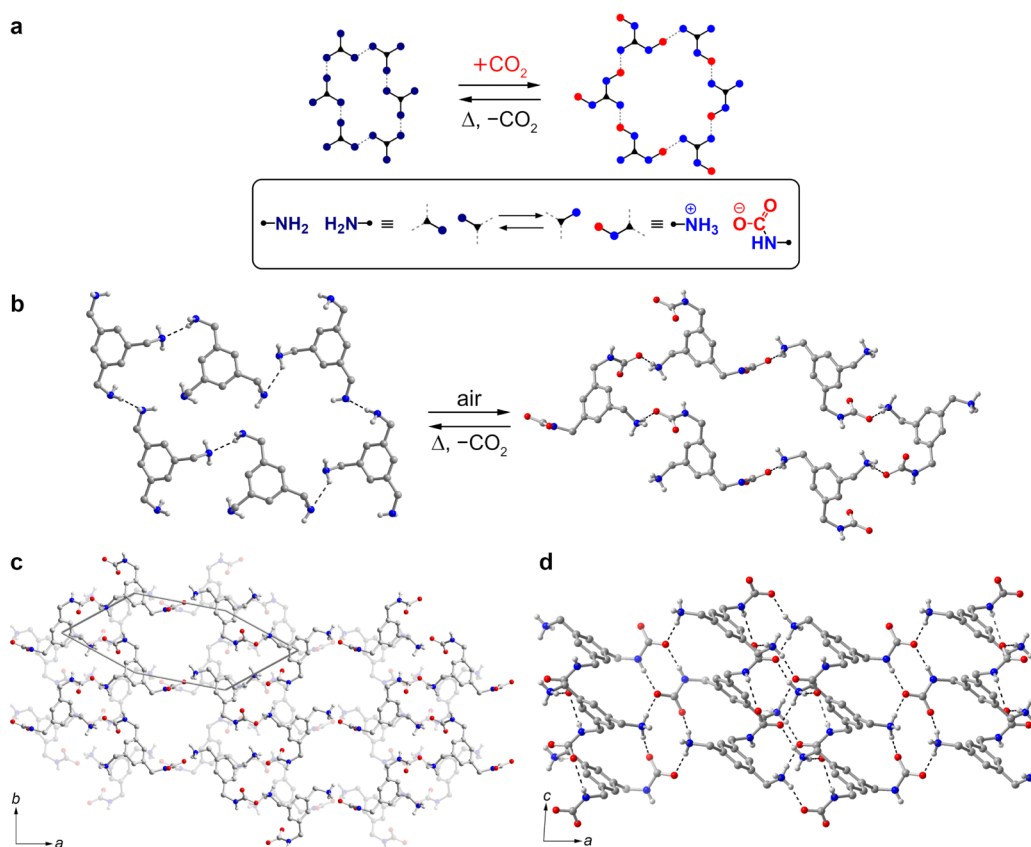


Figure 1. (a) Pictorial representation of ammonium carbamate network formation upon CO_2 insertion with simple, high symmetry, solid molecular polyamines. (b) (Left) Portion of the solid-state structure of TriH obtained from single-crystal X-ray diffraction. Upon exposure to air, TriH ($\text{C}_9\text{H}_{15}\text{N}_3$) chemisorbs CO_2 to form an ammonium carbamate solid TriHCO_2 with a structure resembling a honeycomb net (right). (c) View of a portion of the single-crystal structure of TriHCO_2 along the c -axis, highlighting the stacked two-dimensional sheets. The resulting asymmetric hexagonal pore is highlighted by light gray lines. (d) Through-sheet perspective of TriHCO_2 highlighting hydrogen bonding between sheets. Red, blue, gray, and white spheres represent O, N, C, and H atoms, respectively. Hydrogen bonding interactions are represented by dashed black lines. Aryl and methylene hydrogen atoms are omitted for clarity.

air via reactive crystallization of insoluble hydrogen-bonded frameworks.^{16,21–25} Subsequent isolation of the solid by filtration and desorption of CO_2 regenerates the molecules, which can be redissolved in water for subsequent CO_2 capture. These molecules, in theory, could exhibit some of the highest reported gravimetric CO_2 uptakes under DAC conditions (2.1–4.6 mmol/g), although absorption in a liquid medium imposes inherent diffusional resistance to CO_2 uptake, which is exacerbated by the low concentration of CO_2 in air.²⁶

Owing to their high surface areas and chemical tunability, amine-functionalized metal–organic frameworks^{27–38} and covalent organic frameworks^{39–41} are leading candidates for carbon capture, and some have been shown to adsorb CO_2 at concentrations relevant to those in air with modest to high CO_2 adsorption capacities (1.1–3.9 mmol/g).^{29,31,35,37,39–41} Importantly, the cooperative, ammonium carbamate chain forming mechanism associated with CO_2 uptake in certain diamine- and tetraamine-appended metal–organic frameworks results in stepped adsorption isotherms that require small temperature swings, and therefore lower sensible heat, for regeneration.^{28–30,32,34} Yet, in all such cases, the weight of the supporting framework, which is necessary to imbue these materials with porosity while not directly capturing CO_2 , inherently limits the attainable CO_2 separation capacities.

In view of these challenges, we hypothesized that it might be possible to achieve CO_2 absorption at higher capacities using

simple organic polyamine molecules with no supporting scaffold. Here, a molecule with a rigid core and outwardly directed primary or secondary amine groups might ensure formation of an extended network solid via intermolecular hydrogen bonding (Figure 1a). The insertion of CO_2 between two hydrogen-bonded amine groups to form a hydrogen-bonded ammonium carbamate ion pair would destabilize neighboring hydrogen bonds within the network structure. In such a case, it might be energetically preferable for the entire hydrogen-bonded polyamine solid to convert all at once into an ammonium carbamate network solid through a phase change.

Here, we demonstrate the viability of this strategy with the solid molecular triamine 1,3,5-tris(aminomethyl)benzene (TriH), which rapidly captures CO_2 when exposed to ambient air to generate a porous, crystalline ammonium carbamate network solid. When exposed to simulated air at a range of different global temperatures and relative humidities (RH), TriH exhibits gravimetric CO_2 capacities ranging from ~ 3.3 to 8.9 mmol/g, the latter a record for any sorbent under DAC conditions.

RESULTS AND DISCUSSION

Synthesis of TriH and Initial Characterization of CO_2 Uptake. The molecule TriH was synthesized following a procedure adapted from the literature (see the Supporting

Information for details).⁴² Single-crystals of TriH were prepared under a nitrogen atmosphere by layering diethyl ether over a solution of TriH in methanol. X-ray diffraction analysis of TriH crystals revealed a structure featuring a dense hydrogen bonding network with N(H)⋯N distances ranging from 2.32(2) to 2.64(2) Å (Figures 1b and S27; *Pbca* space group; lattice parameters of $a = 13.8625(13)$ Å, $b = 8.8578(10)$ Å, $c = 14.5071(16)$ Å). Each TriH molecule engages in ten intermolecular hydrogen bonding interactions. Two methylamine moieties rotated out-of-plane with respect to their parent benzene ring engage in hydrogen bonding interactions with amines on adjacent molecules. The in-plane methylamine moiety facilitates orthogonal hydrogen bonding to form two-dimensional amine sheets.

To assess the CO₂ absorption properties of TriH under simple experimental conditions, thermogravimetric analysis (TGA) of TriH was conducted under pure CO₂. The resulting absorption isobar collected for TriH features a sharp step at 53 °C corresponding to a CO₂ absorption capacity of 2.9 mmol/g (Figure 2a). The weight change caused by CO₂ absorption

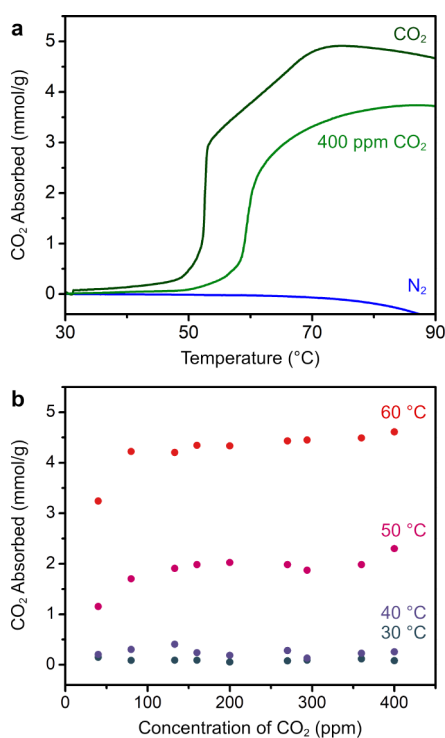


Figure 2. (a) Dry CO₂ absorption isobars for TriH collected under pure CO₂ (dark green) and 400 ppm of CO₂ balanced with N₂ (light green) at ambient pressure. Dry N₂ isobar (blue) is overlaid as a reference. The mass loss under N₂ is attributed to volatilization of TriH. (b) Dry CO₂ absorption capacities for TriH under various concentrations of CO₂ flow (40–400 ppm, N₂ balanced) collected at 30, 40, 50, and 60 °C.

then gradually increases to 5.0 mmol/g as the temperature rises to 75 °C. Interestingly, steep uptake occurs at a temperature near the melting range for TriH (50–52 °C),⁴³ suggesting that melting of TriH may facilitate CO₂ capture under pure CO₂. Isobaric CO₂ absorption data collected for a sample of TriH exposed to flowing dry 400 ppm of CO₂ in N₂—conditions relevant to DAC—reveal stepped CO₂ uptake at 63 °C and a maximum absorbed amount of 3.7 mmol/g at 87 °C (Figure 2a). The increased temperature required for stepped uptake at

400 ppm of CO₂ compared to pure CO₂ reflects an entropy penalty associated with CO₂ absorption at lower concentrations. In contrast to these CO₂ isobars, the TGA data for TriH under pure N₂ do not show an appreciable weight increase upon heating to 70 °C, consistent with the weight change originating from CO₂ absorption. The small weight loss in the TGA curve for TriH under N₂ indicates that TriH begins to volatilize at ~70 °C and rapidly volatilizes at 120 °C (Figure S29), which is attributed to the low molecular weight of TriH, resulting in relatively low melting and boiling points.

To further probe CO₂ uptake, we carried out a series of TGA experiments wherein TriH was exposed to a flowing stream of dilute CO₂ (with concentrations ranging from 40 to 400 ppm) in N₂ at 30, 40, 50, or 60 °C for 24 h. Consistent with the isobaric data, TriH did not absorb appreciable CO₂ at 30 or 40 °C (Figures 2b, S31 and S32). However, at 50 °C and 80 ppm, TriH absorbed 1.7(2) mmol/g (average and standard deviation from duplicate experiments), and this capacity remained relatively constant up to 400 ppm. At 60 °C, the CO₂ uptake nearly doubled over the entire pressure range. Notably, TriH absorbed 4.6 mmol/g when exposed to 400 ppm of CO₂, which is almost the same as the CO₂ uptake observed in the isobar of TriH under a pure CO₂ stream. The dramatic increase in CO₂ uptake by TriH that occurs between 50 and 60 °C is likely facilitated by the onset of TriH melting. Additionally, the kinetics of CO₂ uptake in TriH are highly dependent on the temperature and CO₂ concentration (Figures S31 and S32). For example, uptake of CO₂ at 400 ppm and 50 °C occurs gradually over the course of 24 h, whereas at 60 °C, TriH saturates in approximately 3 h.

X-ray Diffraction Analyses. *In situ* synchrotron powder X-ray diffraction data collected while heating TriH from 20 to 200 °C under dry CO₂ (1 atm) reveals that CO₂ absorption under dry conditions is associated with two distinct phase changes occurring above 50 and 80 °C (Figure 3a). The diffraction pattern obtained at 20 °C reveals a crystalline phase that corresponds to TriH (Figure S19). A Rietveld refinement against powder X-ray diffraction data collected for TriH was performed starting from the TriH structure obtained from single crystal data collected at 100 K, leading to a structure fully consistent with the single crystal structure (Figure S20).

Upon heating to 54 °C, Bragg peaks corresponding to a new second phase begin to grow as the original peaks corresponding to TriH disappear. This first phase transition is consistent with a phase change upon CO₂ absorption. Owing to the broad peak widths in the diffraction pattern, we were unable to determine the structure of the new phase. With further heating above 80 °C, a third phase grows in with the concomitant disappearance of the second phase. This third phase is highly crystalline, and we successfully indexed and performed a Pawley fit against the data collected at 200 °C to extract the unit cell parameters (*P2*₁/*c* space group; lattice parameters of $a = 14.2469(2)$ Å, $b = 8.5126(1)$ Å, $c = 9.0004(1)$ Å, and $\beta = 100.025(1)^\circ$). We hypothesized that the new phase may have a structure in which CO₂ is chemisorbed at only one of the amine sites in each TriH molecule. Accordingly, initial Rietveld refinements of the *P2*₁/*c* structure were attempted (Figure S21) with the rigid body of TriH from a prior Rietveld refinement and modified to substitute two amine groups for one carbamate and one ammonium moiety (Figure 3b).

The higher-temperature phase was successfully identified as a molecular ammonium carbamate network solid of formula

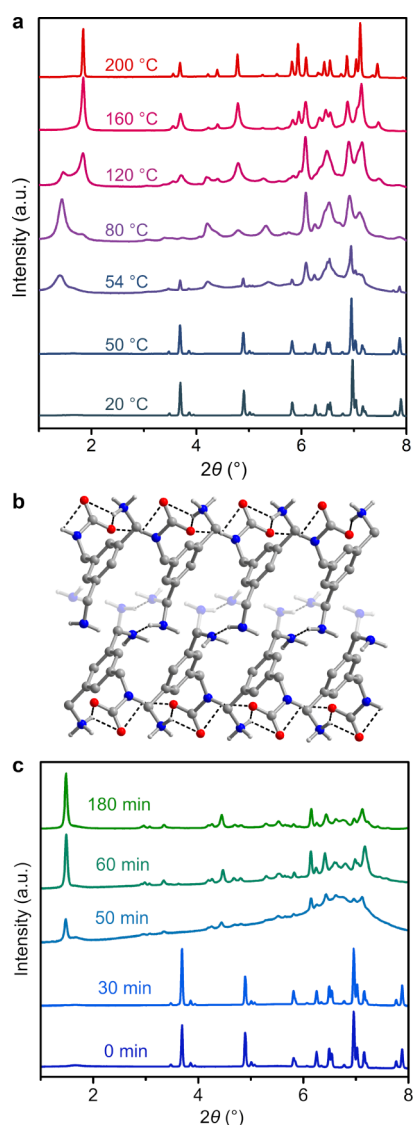


Figure 3. (a) *In situ* variable-temperature powder X-ray diffraction patterns of TriH exposed to pure (1 atm) flowing CO₂ ($\lambda = 0.45207$ Å). At 54 °C, TriH undergoes a phase transition resulting in a second phase with large Bragg peak widths. Another phase transition begins at 120 °C to form a third crystalline phase with sharper Bragg peaks upon heating to 200 °C. (b) Structure of the phase formed after heating a sample of TriH under flowing (1 atm) CO₂ at 200 °C obtained by powder X-ray diffraction. The amine moiety is positionally disordered, and the disordered side chain is shown in paler color. Red, blue, gray, and white spheres represent O, N, C, and H atoms, respectively. Hydrogen atoms not participating in hydrogen bonding are omitted for clarity. Hydrogen bonding interactions are represented by dashed black lines. (c) *In situ* powder X-ray diffraction patterns collected for TriH exposed to air (~35% RH) at 25 °C ($\lambda = 0.45171$ Å).

TriH(CO₂) (C₁₀H₁₅N₃O₂), wherein each molecule features a carbamate group—formed from CO₂ insertion at one amine site—charge-balanced by an adjacent ammonium group (Figure 3b). Together, the oxygen atoms in the carbamate group form four different hydrogen bonds: one intramolecular carbamate-carbamate interaction, one intermolecular carbamate-carbamate nitrogen interaction (O⋯N distance of 2.90(4) Å), and two intermolecular ammonium carbamate interactions (O⋯N bond distances of 2.75(4) and 2.88(3) Å).

Interestingly, the molecules adopt opposing orientations in alternating planes, such that the ammonium and carbamate species interact with ammonium and carbamate species of an adjacent plane. The remaining amine moiety on each molecule engages in hydrogen bonding interactions with amine species on an adjacent plane, resulting in the formation of alternating two-dimensional ammonium carbamate and amine sheets. Additionally, the amine groups of each molecule are positionally disordered, and two different orientations may occur to facilitate hydrogen bonding interactions between adjacent planes. The high-temperature phase may adopt this structure to maximize the number of hydrogen bonding interactions within the lattice.

Additional powder X-ray diffraction experiments were performed with TriH under air to understand the structural behavior of TriH in conditions more relevant to DAC. In contrast to the behavior under dry CO₂, synchrotron powder X-ray diffraction data collected for a sample of TriH exposed to static air at 25 °C changed noticeably after 50 min, as Bragg peaks associated with TriH disappeared and gave way to new reflections (Figure 3c). Additional diffraction patterns collected after 60 and 180 min indicate the phase transition is nearly complete after 60 min. Notably, a Pawley fit against the resulting diffraction pattern revealed a new crystalline phase distinct from that formed under pure CO₂ at elevated temperatures (Figures 3a and S22). The same new phase is also formed upon dosing TriH with 1 atm of humid CO₂, and the transition happens much more rapidly at this higher concentration (Figure S23).

To determine the structure of the new phase, single crystals were grown under ambient air by methanol vapor diffusion into an aqueous solution of air-dosed TriH. X-ray diffraction analysis revealed lattice parameters in agreement with those obtained from a Pawley fit of the humid powder X-ray diffraction data (C2 space group; lattice parameters of $a = 34.2518(10)$ Å, $b = 8.3125(2)$ Å, $c = 9.0798(2)$ Å, and $\beta = 92.799(2)^\circ$). The structure of the air-exposed phase is a three-dimensional hydrogen-bonded porous ammonium carbamate network solid (Figure 1c,d). Here, molecular ions with one (or two) ammonium groups and two (or one) carbamate groups engage in ten intermolecular N(H)⋯O or N(H)⋯N hydrogen bonding interactions with an average proton-acceptor distance of 1.97 Å. The hydrogen bonding interactions along *ab*-plane of the structure result in the formation of honeycomb-like sheets. Additional hydrogen bonding interactions along the *c*-axis stack the honeycomb-like sheets, furnishing a three-dimensional network featuring asymmetric one-dimensional channels (~6 Å × ~3 Å) with a calculated surface area of 500 m²/g (see Supporting Information). The presence of the channels and captured CO₂ molecules contributes to the larger unit cell volume for TriHCO₂ (2587.0(1) vs 1781.3(3) Å³ for TriH). Residual electron density was found in the channels that could not be modeled but is attributed to disordered solvent, supporting the presence of water in the structure formed under humid air. Based on these data, a general formula for the structure formed upon exposure of TriH to humid air is TriH(CO₂)_{1.5}·*x*H₂O (hereafter, “TriHCO₂”). All attempts to completely remove solvent from the pores of TriHCO₂ resulted in a loss of crystallinity, such that the calculated surface area could not be confirmed experimentally (see SI). Nevertheless, the porosity of TriHCO₂ may facilitate the rapid penetration of CO₂ into TriH.

Spectroscopic Characterization of CO₂ Absorption.

Infrared spectroscopy and solid-state NMR spectroscopy were used to further probe the formation of TriHCO₂ upon exposure to air. Time-resolved *in situ* diffuse reflectance infrared Fourier transform spectroscopy (DRIFTS) data were collected for TriH exposed to static air at 20 °C and 35% RH. The resulting infrared spectra exhibited new peaks that near maximum intensity after 30 min (Figure 4). To accurately

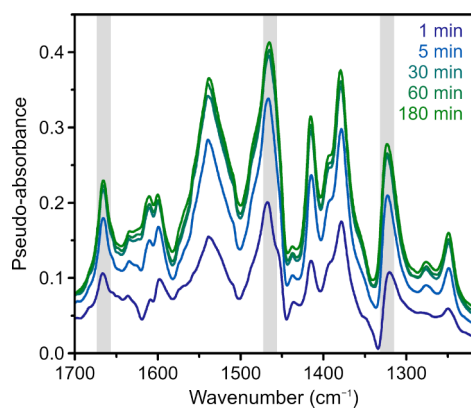


Figure 4. Difference spectra obtained by subtracting *in situ* DRIFTS data collected for TriH upon air exposure at 25 °C. Vibrational modes at 1663, 1464, and 1324 cm⁻¹ for nonenriched TriH (gray bars) are diagnostic for carbamate.³⁴ In the spectrum for TriH (gray trace), the resonance at 1464 cm⁻¹ is assigned to a C–N stretch. This assignment is supported by the data for ¹⁵N-TriH (Figure S16), which revealed a shift in the position of this peak to a lower wavenumber (1456 cm⁻¹).

assign peaks corresponding to carbamate, DRIFTS data were collected for a sample of ¹⁵N-TriH (Figure S16). The peak highlighted at 1464 cm⁻¹ in the TriH spectrum shifts to 1456 cm⁻¹ for ¹⁵N-TriH, confirming its assignment as a carbamate C–N stretch. The additional highlighted vibrations at 1663 and 1324 cm⁻¹ are assigned to carbamate C=O and C–O stretches.^{31,35} These findings clearly support the formation of carbamate species when TriH is exposed to air.

To confirm that both ammonium and carbamate species form when TriH is exposed to air, solid-state magic angle spinning (MAS)¹³C and ¹⁵N NMR spectra were collected for TriHCO₂ (Figure 5). Based on the solution-phase ¹³C chemical shifts of TriH (Figure S2), resonances between 120 and 150 ppm are assigned to aromatic carbons, while resonances between 45 and 50 ppm are assigned to methylene carbons. The resonance at 166.2 ppm for TriHCO₂ is assigned to the carbamate carbon.^{35,44} In the ¹⁵N spectra, each methylamine moiety of TriH gives rise to a unique chemical shift, consistent with the three aminomethyl conformations in the crystal structure of TriH. The spectrum of TriHCO₂ features two peaks corresponding to the carbamate and ammonium nitrogens at 86 and 36 ppm, respectively.

To further support the chemical assignment of the carbamate species, solid-state two-dimensional heteronuclear correlation (HETCOR) spectra were collected for ¹⁵N-labeled TriH dosed at 22 °C with humidified ¹³CO₂ (1 atm). These spectra feature correlations at 6.2 and 166.2 ppm (¹H→¹³C) and 6.2 and 86 ppm (¹H→¹⁵N) (Figure S18), consistent with the previously mentioned carbamate ¹H, ¹³C, and ¹⁵N nuclei assignments. Altogether, the spectroscopic data support the

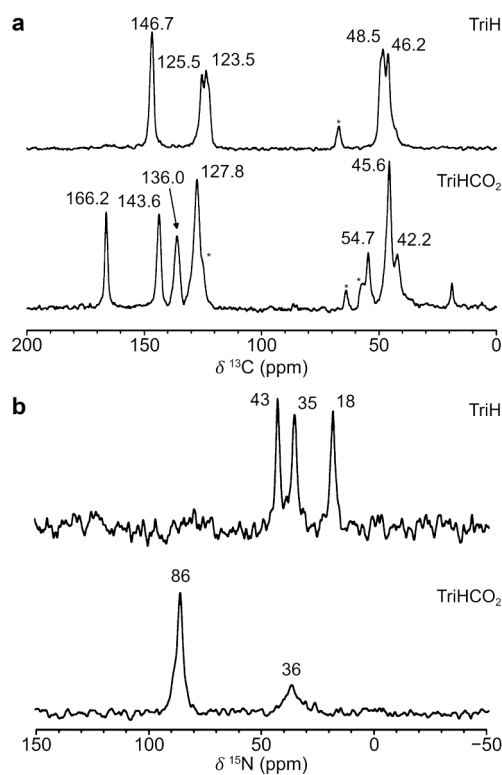


Figure 5. (a) Solid-state MAS ¹³C spectra of TriH and TriHCO₂. The resonance at 166.2 ppm for TriHCO₂ is characteristic of carbamate. Asterisks denote spinning sidebands. (b) Solid-state MAS ¹⁵N spectra of TriH and TriHCO₂. The two resonances at 36 and 86 ppm for TriHCO₂ correspond to ammonium and carbamate nitrogens, respectively.

rapid formation of TriHCO₂ upon direct air capture of CO₂ by TriH.

Carbon Dioxide Uptake under Varying Humidity and Temperature. To evaluate the CO₂ uptake and absorption kinetics of TriH under humid conditions, we utilized a custom-built multicomponent breakthrough analyzer designed to independently quantify absorbed CO₂ and water (Figures S37 and S38). This setup was critical for testing TriH under simulated air at various relative humidities and temperatures reflecting the range of global climates. For a sample of the material exposed to a dry stream of 400 ppm of CO₂ in N₂ flowing at a rate of 50 standard cubic centimeters per minute (sccm) at 20 °C, breakthrough of CO₂ occurred immediately, consistent with the absence of any CO₂ absorption under these conditions (Figure 6a and Table S3). In contrast, at 20% RH and 20 °C, the CO₂ concentration at the outlet gradually increased. After 1,000 min, the solid achieved a CO₂ absorption capacity of 4.6 mmol/g. Increasing the relative humidity of the incident stream from 40% to 80% resulted in greater CO₂ uptakes of 6.0 and 6.4 mmol/g, respectively (Figures 6a and S39).

Powder X-ray diffraction data collected for the sample following breakthrough at 20% RH revealed a new, currently unknown phase (Figure S25). In contrast, under air at ~35% RH, the transition from TriH to TriHCO₂ was complete after ~3 h (Figure 3c). Additionally, powder X-ray diffraction data collected for the sample following breakthrough at 80% RH featured only reflections assignable to TriHCO₂ (Figure S25). Thus, at least under these conditions, relative humidity levels

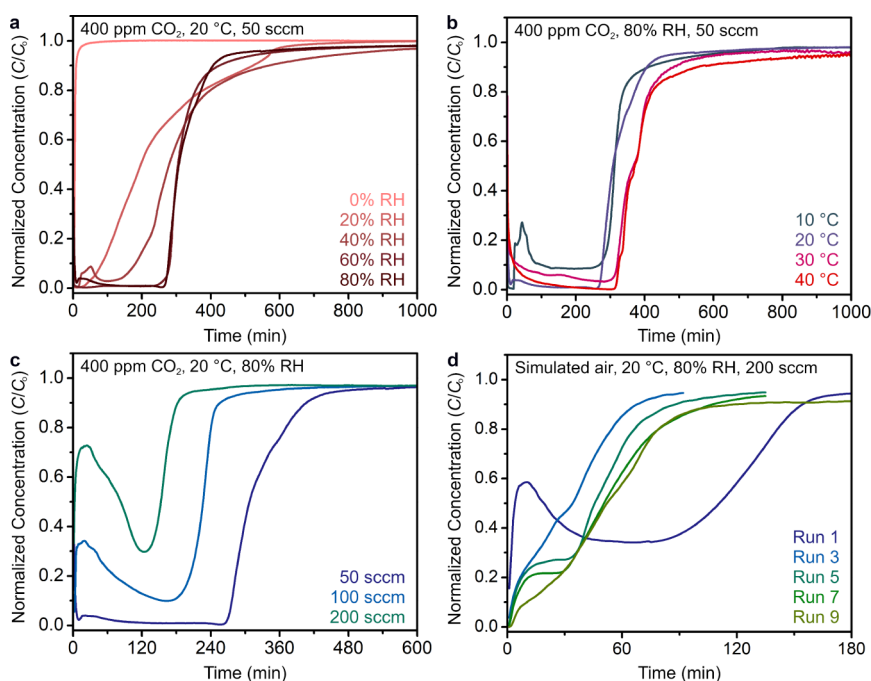


Figure 6. (a) Breakthrough data collected for TriH exposed to a flowing stream of 400 ppm of CO₂ in N₂ at 20 °C and 0, 20, 40, 60, and 80% RH. (b) Breakthrough data collected for TriH exposed to a flowing stream of 400 ppm of CO₂ in N₂ at 80% RH and temperatures of 10, 20, 30, and 40 °C. (c) Breakthrough data collected for TriH exposed to flowing 400 ppm of CO₂ in N₂ at 80% RH and 20 °C with flow rates of 50, 100, and 200 sccm. (d) Selected absorption breakthrough data for TriH collected over the course of absorption–desorption cycling. For each run, the sample was exposed to a flowing stream containing 420 ppm of CO₂ balanced with 21% O₂ and 79% N₂ at 80% RH and 20 °C.

greater than 20% are needed to promote the conversion of TriH to TriHCO₂.

Separate experiments were conducted at 80% RH while varying the temperature between 10 and 40 °C. The breakthrough profiles across this temperature range are all stepped, suggesting that the kinetics of CO₂ absorption by TriH are affected more by relative humidity than by temperature. The CO₂ absorption capacity increased with increasing temperature, ranging from 5.6 to 7.2 mmol/g (Figure 6b and Table S4). Importantly, while CO₂ and water were simultaneously absorbed under all breakthrough conditions, water could be completely desorbed by heating the solid under flowing N₂ at 70 °C (Figure S41) and CO₂ could subsequently be desorbed by heating under flowing N₂ at 110 °C (Figure S42). The regeneration energy to reform TriH from TriHCO₂ was determined using similar conditions (see below).

In a practical DAC process, air flow rates are much higher than those typically measured at the laboratory scale, by at least an order of magnitude.¹⁴ The impact of flow rate on the CO₂ capture properties of TriH was therefore assessed by conducting additional breakthrough experiments with 400 ppm of CO₂ in N₂ at 60% or 80% RH flowing at rates of 100 or 200 sccm at 20 or 40 °C. In general, for a given temperature and relative humidity, faster flow rates were associated with shorter breakthrough times (Table S5). While changing the flow rate had minimal impact on CO₂ capacity at 40 °C, faster flow rates at 20 °C were associated with higher absorption capacities (e.g., 6.1 vs 8.3 mmol/g at 60% RH and 50 and 200 sccm, respectively). This result indicates that CO₂ absorption at 20 °C is kinetically limited. At 100 and 200 sccm, the CO₂ absorption capacities at 20 °C were larger than those at 40 °C, consistent with an entropy penalty associated with CO₂ absorption from the gas phase at higher temperatures.

Significantly, a maximum capacity of 8.9 mmol/g was achieved at 20 °C and 80% RH with a flow rate of 200 sccm (Figure 6c), representing the highest capacity yet reported for any kinetically competent DAC material and approaching the maximum theoretical gravimetric capacity of 9.14 mmol/g for TriH. Based on gravimetric CO₂ uptake alone, the next leading solid DAC material is the amine-appended metal–organic framework N₂H₄–Mg₂(dobdc) (dobdc⁴⁻ = 2,5-dioxido-1,4-benzenedicarboxylate) which exhibits a gravimetric CO₂ uptake of 3.89 mmol/g at 400 ppm of CO₂.²⁷

Regeneration of TriH from TriHCO₂. Given that TriH melts between 50 and 52 °C and volatilizes at 120 °C, it is critical to identify potential operating conditions that minimize or preclude TriH volatilization during regeneration. Relying solely on TGA methods would normally not allow us to distinguish between changes in mass occurring due to desorption rather than volatilization. In order to deconvolute mass loss events, we attached a nondispersive infrared (NDIR) spectrometer at the outlet of the TGA instrument to quantify desorbed CO₂ and water. Over the course of the first 50 min of heating a 2.53 mg sample of TriHCO₂ at 100 °C, a total mass loss of 0.74 mg was measured (Figure 7a). In parallel, the calculated quantity of CO₂ and water desorbed based on NDIR measurements were 0.53 (~84% of the absorbed CO₂) and 0.22 mg, respectively, summing to 0.75 mg of desorbed species (Figure 7b). As the TGA and NDIR data are in good agreement, we conclude that only desorption occurred in the first 50 min of heating at 100 °C, with no loss of TriH. In the following 250 min, small amounts of CO₂ and water were desorbed (0.09 and 0.03 mg, respectively), while the sample mass as measured by TGA continued to decrease by 0.67 mg. The majority of this later mass loss (0.55 mg = 0.67 – 0.09 – 0.03 mg) can thus be attributed to volatilization of TriH. While prolonged heating of TriHCO₂ may induce volatilization, these

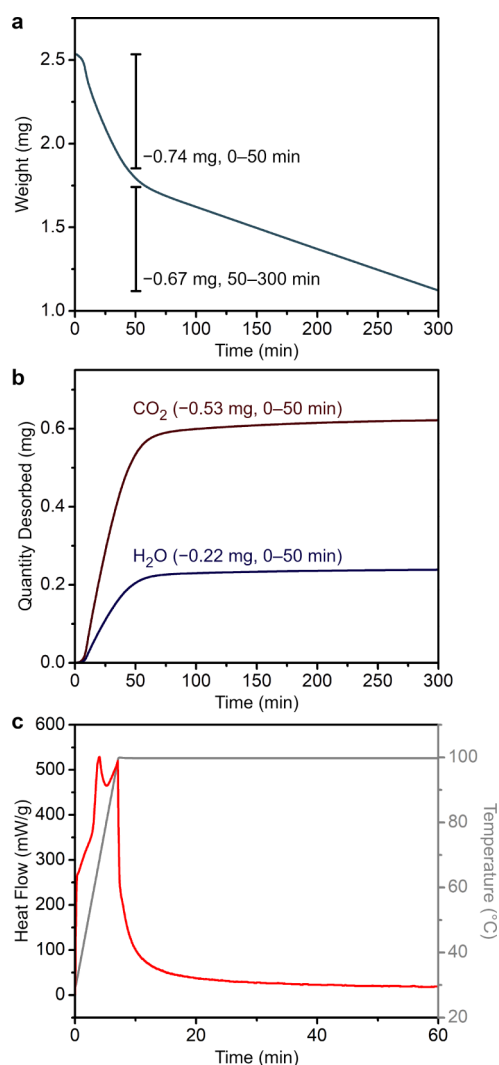


Figure 7. (a) Weight loss over time for a sample of TriHCO_2 (2.53 mg) held at $100\text{ }^\circ\text{C}$ for 5 h under flowing N_2 (25 mL/min) in a thermogravimetric analyzer. (b) Quantities of CO_2 and water desorbed from TriHCO_2 determined by NDIR during the same weight loss experiment. Mass loss within the first 50 min is due exclusively to desorption of CO_2 and water. Mass loss after 50 min is due to a combination of desorption and volatilization of TriH . (c) Differential scanning calorimetry data collected for TriHCO_2 under flowing (25 mL/min) N_2 . The data were integrated over time to estimate the energy required to regenerate TriH from TriHCO_2 , which was 292 J/g (74.0 kJ/mol).

data suggest the possibility of suppressing volatilization with short desorption periods.

The previous experiment suggests that the regeneration energy of TriH from TriHCO_2 can be estimated by assuming that only CO_2 and water desorption occurs when maintaining TriHCO_2 at $100\text{ }^\circ\text{C}$ under N_2 . To quantify the energy required to partially regenerate TriH from TriHCO_2 (while limiting TriH volatilization), we conducted differential scanning calorimetry measurements under conditions analogous to the previous NDIR experiment (Figure 7c). The energy required to regenerate TriH from TriHCO_2 is composed of the sensible heat (i.e., the energy required to heat TriHCO_2 from 20 to $100\text{ }^\circ\text{C}$) and the enthalpy of desorption (estimated as the energy required to desorb CO_2 and water from TriHCO_2 while at $100\text{ }^\circ\text{C}$ for 50 min). The calculated sensible heat for the first 8 min

as TriHCO_2 was heated from 20 to $100\text{ }^\circ\text{C}$ is 170 J/g (43.1 kJ/mol TriH). We note that minimal amounts of CO_2 and water indeed desorb while heating TriHCO_2 to $100\text{ }^\circ\text{C}$, so the sensible heat and enthalpy of desorption may be slightly overestimated and underestimated, respectively. The enthalpy of desorption (of CO_2 and water) is calculated to be 122 J/g (30.9 kJ/mol TriH) for the subsequent 50 min where TriHCO_2 was maintained at $100\text{ }^\circ\text{C}$. From these data, we estimated a lower bound for the regeneration energy of 292 J/g (74.0 kJ/mol TriH), consistent with that determined for other amine-based sorbents that form ammonium carbamates upon CO_2 capture.³² We note that this is a lower bound because the sample was heated to desorb only $\sim 90\%$ of the CO_2 and water to preclude TriH volatilization.

Absorption–Desorption Cycling. The CO_2 capture performance of TriH was followed over the course of repeated absorption–desorption cycles to better assess its potential for DAC. To monitor the degree of sample volatilization during cycling, breakthrough data and subsequent desorption data were collected using a glass breakthrough column. Absorption data were collected under a 200-sccm flow of 400 ppm of CO_2 in N_2 at 80% RH and $20\text{ }^\circ\text{C}$, and desorption data were collected while flowing N_2 at $110\text{ }^\circ\text{C}$ (Figures S55 and S56). Under these conditions, TriH was observed to at least partially dissolve in absorbed water within ~ 2 min of exposure to the gas stream, followed by subsequent CO_2 uptake and formation of solid TriHCO_2 after ~ 20 min or less. We note that, while TriH deliquesces during absorption, excess water is then vaporized as solid TriHCO_2 forms, which is a behavior unlike the aqueous amine and iminoguanidine solutions. Upon switching to flowing N_2 for desorption, condensation downstream of the sample corresponding to water desorption was observed within the glass breakthrough column in the first 2 min, while, beginning at ~ 20 min, a visible solid was observed downstream of the column, indicative of TriH volatilization.

The results from the previous experiments suggest that it should be possible to suppress volatilization of TriH by minimizing the desorption time. Based on these results, cycling experiments were conducted using our custom breakthrough column setup with absorption at $20\text{ }^\circ\text{C}$ under a flowing (200 sccm) gas stream containing 420 ppm of CO_2 , 21% O_2 , and 79% N_2 at 80% RH (Figures 6d and S49) and desorption under flowing (100 sccm) dry N_2 at $110\text{ }^\circ\text{C}$ for only ~ 13 min (Figure S50). In the first absorption run, TriH absorbed $6.0\text{ mmol CO}_2/\text{g}$ and exhibited a similar breakthrough profile and CO_2 uptake to the data collected under humid 400 ppm of CO_2 at 80% RH and 200 sccm after 3 h (Figure 6c). We note that this result indicates that O_2 does not significantly impact CO_2 uptake under these conditions. Additional oxidative stability experiments (see Figures S15, S35 and S36) further confirm the oxidative robustness and long-term stability of TriHCO_2 . Following the first absorption run, only $1.8\text{ mmol CO}_2/\text{g}$ were recovered in the first desorption run, and the same quantity of CO_2 was subsequently captured in the second absorption run. Surprisingly, however, 2.4 mmol/g was recovered in the subsequent desorption run. The quantity of CO_2 absorbed generally continued to increase until the ninth cycle (to 4.5 mmol/g), and the quantity of CO_2 desorbed increased to 4.1 mmol/g after the fifth cycle, and then fluctuated between 3.3 and 4.4 mmol/g in the later cycles (Table S6). We hypothesize that deliquescence of TriH in the early cycles led to coating of the solid in the breakthrough column, which may have facilitated subsequent CO_2 uptake

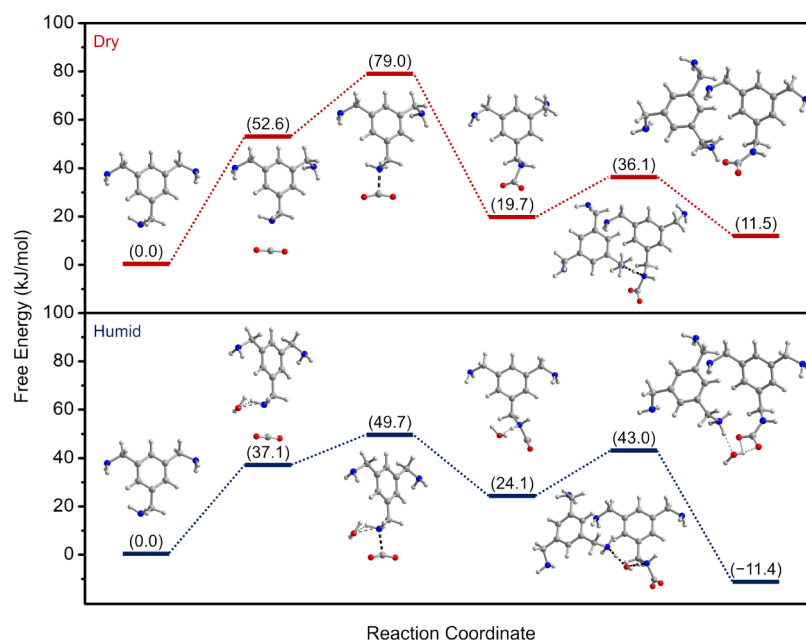


Figure 8. Calculated free energy landscapes for CO₂ absorption in TriH under dry and humid conditions. (Upper) Dry conditions: free energy calculations were performed using ten TriH molecules and one CO₂ molecule with the reactive amine site encapsulated in the center of the cluster. (Lower) Humid conditions: free energy calculations were performed using ten TriH molecules, one CO₂ molecule, and one water molecule with the reactive amine encapsulated in the center of the cluster. Inclusion of one water molecule introduces additional hydrogen bonding interactions, lowering the first transition state energy relative to that under dry conditions. Dashed gray lines denote intermolecular hydrogen bonding interactions. Dashed black lines denote the making or breaking of bonds.

and recovery (Figure S50). This factor, as well as the limited thermal stability of TriH, could contribute to the fluctuations in CO₂ uptake throughout the ten absorption–desorption cycles.

Free Energy Landscape for Dry and Humid CO₂ Uptake. Since the presence of humidity significantly increases CO₂ uptake in TriH, we sought to gain mechanistic insight toward the role of water in CO₂ absorption. We hypothesized that water may lower the activation barrier for CO₂ absorption by stabilizing the transition state for N–C bond formation via hydrogen bonding interactions and/or directly participating as a proton transfer mediator during ammonium carbamate formation. To explore these possibilities, we carried out density functional theory (DFT) calculations to assess the free energy landscape for CO₂ absorption under dry and humid conditions, using models generated from the single crystal structure of TriH (Figures S57–S67).

Based on the study of the solid-state reaction between CO₂ and ammonia,⁴⁵ CO₂ uptake was modeled by first inserting CO₂ into an amine group of TriH to generate a metastable zwitterionic ammonium carbamate (Figure 8, upper). A neighboring TriH molecule then abstracts a proton from the zwitterion to generate an ammonium ion that pairs with the resulting carbamate. Under dry conditions, the activation energy associated with CO₂ addition is 79.0 kJ/mol, which suggests that this reaction should be slow near ambient temperatures. In addition, the overall reaction to form an ammonium carbamate is endergonic ($\Delta G = +11.5$ kJ/mol), consistent with the lack of uptake observed in dry CO₂ absorption experiments. Under humid conditions, the activation energy for CO₂ addition is only 49.7 kJ/mol (Figure 8, lower). While the entropy penalty for CO₂ addition is greater under humid conditions due to reorganization of a nearby water molecule, hydrogen bonding interactions

between the ammonium cation and a water molecule result in an enthalpic stabilization that gives rise to a lower overall activation barrier. Water subsequently serves as a proton transfer mediator by abstracting a proton from the zwitterion while it is simultaneously deprotonated by a neighboring TriH molecule. Consistent with the observed propensity of TriH for CO₂ capture, the overall reaction is now exergonic ($\Delta G = -11.4$ kJ/mol) owing to hydrogen bonding interactions of the water molecule with both the ammonium cation and the carbamate anion.

Notably, the calculated lattice energy of TriH is substantially lower in magnitude than that of TriHCO₂ (-67.3 vs -450.8 kJ/mol), which suggests that the TriHCO₂ network is much more stable. This greater stability is likely due in part to the shorter, therefore stronger, hydrogen bonding interactions in TriHCO₂ vs TriH (average N(H)⋯O and N(H)⋯N distances of 1.97 and 2.44 Å, respectively; Figure 1b).

CONCLUSIONS AND OUTLOOK

The foregoing results show that the solid molecular polyamine TriH (1,3,5-tris(aminomethyl)benzene) can selectively and rapidly capture large quantities of CO₂ from air. X-ray diffraction analyses reveal that TriH undergoes a unique crystalline phase transition upon exposure to static air to generate the porous ammonium carbamate solid TriHCO₂. The formation of an ammonium carbamate species upon dosing TriH with air was also confirmed by DRIFTS and solid-state NMR analyses. In the absence of water, TriH does not absorb appreciable quantities of CO₂ until it is heated to 50 °C, which is near the melting point of TriH. In contrast, breakthrough experiments revealed that, under humid air, TriH can exhibit CO₂ absorption capacities as high as 8.9 mmol/g of CO₂—the highest reported to date for any DAC material. DFT analysis reveals that water stabilizes the

transition state associated with N–C bond formation via hydrogen bonding interactions while also stabilizing the ultimate ammonium carbamate product. Importantly, TriH maintains a high capacity over the course of repeated cycling under simulated humid air at 20 °C.

Our findings establish the exciting prospect of developing lightweight crystalline polyamines for the rapid, high-capacity capture of CO₂ from the atmosphere. We envision multiple possible avenues to circumvent some of the challenges of this proof-of-concept system, including the design of heavier polyamines that are less volatile and maintain stable breakthrough profiles throughout repeated cycles. Alternatively, the use of alternative regeneration schemes, such as microwave-assisted regeneration,⁴⁶ may circumvent the risk of volatilization inherent with a more traditional temperature swing process. Furthermore, the inherent tunability of these molecules suggests the broad applicability of molecular polyamines for CO₂ capture from a range of point source emissions.

■ ASSOCIATED CONTENT

SI Supporting Information

The Supporting Information is available free of charge at <https://pubs.acs.org/doi/10.1021/jacs.4c18643>.

Detailed experimental procedures, synthetic procedures, and characterization data, *in situ* diffuse reflectance infrared spectroscopy data, solid-state NMR data, X-ray crystallographic information, surface area measurements data, thermogravimetric analysis data, breakthrough measurements data, and computational information (PDF)

Accession Codes

Deposition Numbers 2294595 and 2296617–2296618 contain the supplementary crystallographic data for this paper. These data can be obtained free of charge via the joint Cambridge Crystallographic Data Centre (CCDC) [Access Structures service](#).

■ AUTHOR INFORMATION

Corresponding Author

Jeffrey R. Long – *Institute for Decarbonization Materials, University of California, Berkeley, California 94720, United States; Department of Chemistry, Department of Chemical and Biomolecular Engineering, and Department of Materials Science and Engineering, University of California, Berkeley, California 94720, United States; Materials Sciences Division, Lawrence Berkeley National Laboratory, Berkeley, California 94720, United States; orcid.org/0000-0002-5324-1321; Email: jrlong@berkeley.edu*

Authors

Adrian J. Huang – *Institute for Decarbonization Materials, University of California, Berkeley, California 94720, United States; Department of Chemistry, University of California, Berkeley, California 94720, United States; Materials Sciences Division, Lawrence Berkeley National Laboratory, Berkeley, California 94720, United States*

Ankur K. Gupta – *Institute for Decarbonization Materials, University of California, Berkeley, California 94720, United States; Applied Mathematics and Computational Research Division, Lawrence Berkeley National Laboratory, Berkeley,*

California 94720, United States; orcid.org/0000-0002-3128-9535

Henry Z. H. Jiang – *Institute for Decarbonization Materials, University of California, Berkeley, California 94720, United States; Department of Chemistry, University of California, Berkeley, California 94720, United States; Materials Sciences Division, Lawrence Berkeley National Laboratory, Berkeley, California 94720, United States*

Hao Zhuang – *Institute for Decarbonization Materials, University of California, Berkeley, California 94720, United States; Department of Chemical and Biomolecular Engineering, University of California, Berkeley, California 94720, United States*

Malia B. Wenny – *Center for Neutron Research, National Institute of Standards and Technology, Gaithersburg, Maryland 20899, United States; orcid.org/0000-0002-0704-8184*

Ryan A. Klein – *Center for Neutron Research, National Institute of Standards and Technology, Gaithersburg, Maryland 20899, United States; Materials, Chemical, and Computational Sciences Directorate, National Renewable Energy Laboratory, Golden, Colorado 80401, United States*

Hyunchul Kwon – *Institute for Decarbonization Materials, University of California, Berkeley, California 94720, United States; Department of Chemistry, University of California, Berkeley, California 94720, United States*

Katie R. Meihaus – *Institute for Decarbonization Materials, University of California, Berkeley, California 94720, United States; Department of Chemistry, University of California, Berkeley, California 94720, United States*

Hiroyasu Furukawa – *Institute for Decarbonization Materials, University of California, Berkeley, California 94720, United States; Department of Chemistry, University of California, Berkeley, California 94720, United States; Materials Sciences Division, Lawrence Berkeley National Laboratory, Berkeley, California 94720, United States; orcid.org/0000-0002-6082-1738*

Craig M. Brown – *Center for Neutron Research, National Institute of Standards and Technology, Gaithersburg, Maryland 20899, United States; Department of Chemical and Biomolecular Engineering, University of Delaware, Newark, Delaware 19716, United States; orcid.org/0000-0002-9637-9355*

Jeffrey A. Reimer – *Institute for Decarbonization Materials, University of California, Berkeley, California 94720, United States; Materials Sciences Division, Lawrence Berkeley National Laboratory, Berkeley, California 94720, United States; Department of Chemical and Biomolecular Engineering, University of California, Berkeley, California 94720, United States*

Wibe A. de Jong – *Institute for Decarbonization Materials, University of California, Berkeley, California 94720, United States; Applied Mathematics and Computational Research Division, Lawrence Berkeley National Laboratory, Berkeley, California 94720, United States; orcid.org/0000-0002-7114-8315*

Complete contact information is available at: <https://pubs.acs.org/doi/10.1021/jacs.4c18643>

Notes

The authors declare the following competing financial interest(s): The University of California, Berkeley has applied

for a patent on some of the technology discussed herein regarding direct air capture of CO₂ with polyamines, on which A.J.H. and J.R.L. are listed as co-inventors.

ACKNOWLEDGMENTS

This work was supported by the U.S. Department of Energy (DOE), Office of Science, Basic Energy Sciences, Materials Sciences and Engineering Division under Contract No. DE-AC02-05CH11231, FWP No. DAC-LBL-Long. This research used resources of the Advanced Light Source, which is a DOE Office of Science User Facility under contract no. DE-AC02-05CH11231. Crystallographic studies of TriH were carried out at beamline 12.2.1. We thank Dr. Simon Teat for technical assistance with single-crystal X-ray diffraction data collection and refinement. This research used resources of the Advanced Photon Source, a U.S. DOE Office of Science user facility operated for the DOE Office of Science by Argonne National Laboratory under Contract No. DE-AC02-06CH11357. Powder X-ray diffraction data of TriH were carried out at beamline 17-BM-B. We thank Dr. Andrey Yakovenko for technical assistance with powder X-ray diffraction data collection and refinement. This work was partially supported by the NIST Center for Neutron Research (M.B.W., C.M.B.) and the National Research Council of the United States of America through the Research Associate Program (M.B.W.). We further acknowledge fellowship support for A.J.H. from the National Science Foundation Graduate Research Fellowship program and support of J.R.L. by the Miller Institute for Basic Research in Science at the University of California, Berkeley. R.A.K. gratefully acknowledges from the U.S. DOE Office of Energy Efficiency and Renewable Energy, Hydrogen and Fuel Cell Technologies Office, contract no. DE-AC36-8G028308 to the National Renewable Energy Laboratory. We thank Dr. Matthew N. Dods and Dr. Kurtis M. Carsch for helpful discussions and assistance with experimental design. We thank Drs. Hasan Celik, Raynald Giovine, and Pines Magnetic Resonance Center's Core NMR Facility (PMRC Core) for spectroscopic assistance. The instruments used in this work were supported by the PMRC Core.

REFERENCES

- (1) Socolow, R.; Desmond, M.; Aines, R.; Blackstock, J.; Bolland, O.; Kaarsberg, T.; Lewis, N.; Mazzotti, M.; Pfeffer, A.; Sawyer, K., et al. *Direct Air Capture of CO₂ with Chemicals: A Technology Assessment for the APS Panel on Public Affairs*, American Physical Society: College Park, MD, 2011.
- (2) Rogelj, J.; Schaeffer, M.; Meinshausen, M.; Knutti, R.; Alcamo, J.; Riahi, K.; Hare, W. Zero Emission Targets as Long-Term Global Goals for Climate Protection. *Environ. Res. Lett.* **2015**, *10*, No.105007.
- (3) Davis, S. J.; Lewis, N. S.; Shaner, M.; Aggarwal, S.; Arent, D.; Azevedo, I. L.; Benson, S. M.; Bradley, T.; Brouwer, J.; Chiang, Y.-M.; et al. Net-zero Emissions Energy Systems. *Science* **2018**, *360*, No. eaas9793.
- (4) Azarabadi, H.; Lackner, K. S. A Sorbent-Focused Techno-Economic Analysis of Direct Air Capture. *Appl. Energy* **2019**, *250*, 959–975.
- (5) Artz, J.; Müller, T. E.; Thenert, K.; Kleinekorte, J.; Meys, R.; Sternberg, A.; Bardow, A.; Leitner, W. Sustainable Conversion of Carbon Dioxide: An Integrated Review of Catalysis and Life Cycle Assessment. *Chem. Rev.* **2018**, *118*, 434–504.
- (6) Kätelhön, A.; Meys, R.; Deutz, S.; Suh, S.; Bardow, A. Climate Change Mitigation Potential of Carbon Capture and Utilization in the Chemical Industry. *Proc. Natl. Acad. Sci. U. S. A.* **2019**, *116*, 11187–11194.
- (7) The International Energy Agency. *Direct Air Capture 2022 – Analysis*. <https://www.iea.org/reports/direct-air-capture-2022>. (accessed 13 February 2025).
- (8) Matthews, H. D.; Caldeira, K. Stabilizing Climate Requires Near-Zero Emissions. *Geophys. Res. Lett.* **2008**, *35*, No. L04705.
- (9) National Academies of Sciences, Engineering, and Medicine. *Negative Emissions Technologies and Reliable Sequestration: A Research Agenda*; National Academies Press: Washington DC, 2019.
- (10) Masson-Delmotte, V.; Zhai, P.; Pirani, A.; Connors, S.; Péan, C.; Berger, S.; Caud, N.; Chen, Y.; Goldfarb, L.; Gomis, M., et al. *Climate Change 2021: The Physical Science Basis: Contribution of Working Group I to the Sixth Assessment Report of the Intergovernmental Panel on Climate Change*, Cambridge University Press, Cambridge, United Kingdom and New York, NY, USA, 2021.
- (11) The White House. *Executive Order on Catalyzing Clean Energy Industries and Jobs through Federal Sustainability*. 2021. <https://www.federalregister.gov/documents/2021/12/13/2021-27114/catalyzing-clean-energy-industries-and-jobs-through-federal-sustainability>. (accessed 13 February 2024).
- (12) Husk, J. C.; Wenz, G. B. Inside-Out: Driving Down Direct Air Capture Costs with High-Efficiency Adsorbents. *Front. Clim.* **2022**, *3*, No. 787500.
- (13) Smith, S. M.; Geden, O.; Nemet, G.; Gidden, M.; Lamb, W. F.; Powis, C.; Bellamy, R.; Callaghan, M.; Cowie, A.; Cox, E. et al. *The State of Carbon Dioxide Removal – The State of Carbon Dioxide Removal*, 1st ed.; GEOMAR, 2023.
- (14) Keith, D. W.; Holmes, G.; St. Angelo, D.; Heidel, K. A Process for Capturing CO₂ from the Atmosphere. *Joule* **2018**, *2*, 1573–1594.
- (15) Shi, X.; Xiao, H.; Azarabadi, H.; Song, J.; Wu, X.; Chen, X.; Lackner, K. S. Sorbents for the Direct Capture of CO₂ from Ambient Air. *Angew. Chem., Int. Ed.* **2020**, *59*, 6984–7006.
- (16) Gebald, C.; Wurzbacher, J. A.; Tingaut, P.; Zimmermann, T.; Steinfeld, A. Amine-Based Nanofibrillated Cellulose as Adsorbent for CO₂ Capture from Air. *Environ. Sci. Technol.* **2011**, *45*, 9101–9108.
- (17) Didas, S. A.; Choi, S.; Chaikittisilp, W.; Jones, C. W. Amine–Oxide Hybrid Materials for CO₂ Capture from Ambient Air. *Acc. Chem. Res.* **2015**, *48*, 2680–2687.
- (18) Custelcean, R. Direct Air Capture of CO₂ via Crystal Engineering. *Chem. Sci.* **2021**, *12*, 12518–12528.
- (19) Deutz, S.; Bardow, A. Life-Cycle Assessment of an Industrial Direct Air Capture Process Based on Temperature–Vacuum Swing Adsorption. *Nat. Energy* **2021**, *6*, 203–213.
- (20) Seipp, C. A.; Williams, N. J.; Kidder, M. K.; Custelcean, R. CO₂ Capture from Ambient Air by Crystallization with a Guanidine Sorbent. *Angew. Chem., Int. Ed.* **2017**, *56*, 1042–1045.
- (21) Brethomé, F. M.; Williams, N. J.; Seipp, C. A.; Kidder, M. K.; Custelcean, R. Direct Air Capture of CO₂ via Aqueous-Phase Absorption and Crystalline-Phase Release Using Concentrated Solar Power. *Nat. Energy* **2018**, *3*, 553–559.
- (22) Custelcean, R.; Williams, N. J.; Garrabrant, K. A.; Agullo, P.; Brethomé, F. M.; Martin, H. J.; Kidder, M. K. Direct Air Capture of CO₂ with Aqueous Amino Acids and Solid Bis-iminoguanidines (BIGs). *Ind. Eng. Chem. Res.* **2019**, *58*, 23338–23346.
- (23) Williams, N. J.; Seipp, C. A.; Brethomé, F. M.; Ma, Y.-Z.; Ivanov, A. S.; Bryantsev, V. S.; Kidder, M. K.; Martin, H. J.; Holguin, E.; Garrabrant, K. A.; Custelcean, R. CO₂ Capture via Crystalline Hydrogen-Bonded Bicarbonate Dimers. *Chem* **2019**, *5*, 719–730.
- (24) Cai, H.; Zhang, X.; Lei, L.; Xiao, C. Direct CO₂ Capture from Air via Crystallization with a Trichelating Iminoguanidine Ligand. *ACS Omega* **2020**, *5*, 20428–20437.
- (25) Sabatino, F.; Grimm, A.; Gallucci, F.; van Sint Annaland, M.; Jan Kramer, G.; Gazzani, M. A Comparative Energy and Costs Assessment and Optimization for Direct Air Capture Technologies. *Joule* **2021**, *5*, 2047–2076.
- (26) Kiani, A.; Jiang, K.; Feron, P. Techno-Economic Assessment for CO₂ Capture from Air Using a Conventional Liquid-Based Absorption Process. *Front. Energy Res.* **2020**, *8*, No. 92.
- (27) Vaidhyanathan, R.; Iremonger, S. S.; Dawson, K. W.; Shimizu, G. K. H. An Amine-Functionalized Metal Organic Framework for

Preferential CO₂ Adsorption at Low Pressures. *Chem. Commun.* **2009**, 5230–5232.

(28) McDonald, T. M.; Lee, W. R.; Mason, J. A.; Wiers, B. M.; Hong, C. S.; Long, J. R. Capture of Carbon Dioxide from Air and Flue Gas in the Alkylamine-Appended Metal–Organic Framework Mmen-Mg₂(dobpdc). *J. Am. Chem. Soc.* **2012**, *134*, 7056–7065.

(29) Lee, W. R.; Hwang, S. Y.; Ryu, D. W.; Lim, K. S.; Han, S. S.; Moon, D.; Choi, J.; Hong, C. S. Diamine-Functionalized Metal–Organic Framework: Exceptionally High CO₂ Capacities from Ambient Air and Flue Gas, Ultrafast CO₂ Uptake Rate, and Adsorption Mechanism. *Energy Environ. Sci.* **2014**, *7*, 744–751.

(30) McDonald, T.; Mason, J. A.; Kong, X.; Bloch, E. D.; Gygi, D.; Dani, A.; Crocellà, V.; Giordanino, F.; Odoh, S. O.; Drisdell, W. S.; Vlasisavljevič, B.; Dzubak, A. L.; Poloni, R.; Schnell, S. K.; Planas, N.; Lee, K.; Pascal, T.; Wan, L. F.; Prendergast, D.; Neaton, J. B.; Smit, B.; Kortright, J. B.; Gagliardi, L.; Bordiga, S.; Reimer, J. A.; Long, J. R. Cooperative Insertion of CO₂ in Diamine-Appended Metal–Organic Frameworks. *Nature* **2015**, *519*, 303–308.

(31) Liao, P.-Q.; Chen, X.-W.; Liu, S.-Y.; Li, X.-Y.; Xu, Y.-T.; Tang, M.; Rui, Z.; Ji, H.; Zhang, J.-P.; Chen, X.-M. Putting an Ultrahigh Concentration of Amine Groups into a Metal–Organic Framework for CO₂ Capture at Low Pressures. *Chem. Sci.* **2016**, *7*, 6528–6533.

(32) Siegelman, R. L.; McDonald, T. M.; Gonzalez, M. I.; Martell, J. D.; Milner, P. J.; Mason, J. A.; Berger, A. H.; Bhowan, A. S.; Long, J. R. Controlling Cooperative CO₂ Adsorption in Diamine-Appended Mg₂(dobpdc) Metal–Organic Frameworks. *J. Am. Chem. Soc.* **2017**, *139*, 10526–10538.

(33) Darunte, L. A.; Terada, Y.; Murdock, C. R.; Walton, K. S.; Sholl, D. S.; Jones, C. W. Monolith-Supported Amine-Functionalized Mg₂(dobpdc) Adsorbents for CO₂ Capture. *ACS Appl. Mater. Interfaces* **2017**, *9*, 17042–17050.

(34) Kim, E. J.; Siegelman, R. L.; Jiang, H. Z. H.; Forse, A. C.; Lee, J.-H.; Martell, J. D.; Milner, P. J.; Falkowski, J. M.; Neaton, J. B.; Reimer, J. A.; Weston, S. C.; Long, J. R. Cooperative Carbon Capture and Steam Regeneration with Tetraamine-Appended Metal–Organic Frameworks. *Science* **2020**, *369*, 392–396.

(35) Park, J.; Park, J. R.; Choe, J. H.; Kim, S.; Kang, M.; Kang, D. W.; Kim, J. Y.; Jeong, Y. W.; Hong, C. S. Metal–Organic Framework Adsorbent for Practical Capture of Trace Carbon Dioxide. *ACS Appl. Mater. Interfaces* **2020**, *12*, 50534–50540.

(36) Justin, A.; Espin, J.; Kochetygov, I.; Asgari, M.; Trukhina, O.; Queen, W. L. A Two Step Postsynthetic Modification Strategy: Appending Short Chain Polyamines to Zn-NH₂-BDC MOF for Enhanced CO₂ Adsorption. *Inorg. Chem.* **2021**, *60*, 11720–11729.

(37) Chen, O. I.-F.; Liu, C.-H.; Wang, K.; Borrego-Marin, E.; Li, H.; Alawadhi, A. H.; Navarro, J. A. R.; Yaghi, O. M. Water-Enhanced Direct Air Capture of Carbon Dioxide in Metal–Organic Frameworks. *J. Am. Chem. Soc.* **2024**, *146*, 2835–2844.

(38) Justin, A.; Espin, J.; Pougin, M. J.; Stoian, D.; Schertenleib, T.; Mensi, M.; Kochetygov, I.; Ortega-Guerrero, A.; Queen, W. L. Post-Synthetic Covalent Grafting of Amines to NH₂-MOF for Post-Combustion Carbon Capture. *Adv. Funct. Mater.* **2024**, *34*, No. 2307430.

(39) Lyu, H.; Li, H.; Hanikel, N.; Wang, K.; Yaghi, O. Covalent Organic Frameworks for Carbon Dioxide Capture from Air. *J. Am. Chem. Soc.* **2022**, *144*, 12989–12995.

(40) Zhou, Z.; Ma, T.; Zhang, H.; Chheda, S.; Li, H.; Wang, K.; Ehrling, S.; Giovine, R.; Li, C.; Alawadhi, A. H.; et al. Carbon Dioxide Capture from Open Air Using Covalent Organic Frameworks. *Nature* **2024**, *635*, 96–101.

(41) Li, H.; Zhou, Z.; Ma, T.; Wang, K.; Zhang, H.; Alawadhi, A.; Yaghi, O. M. Bonding of Polyethylenimine in Covalent Organic Frameworks for CO₂ Capture from Air. *J. Am. Chem. Soc.* **2024**, *146*, 35486–35492.

(42) López-Ruiz, H.; Cortés-Hernández, M.; Rojas-Lima, S.; Höpfl, H. Synthesis of Nitrogen-, Oxygen- and Sulphur-Containing Tripodal Ligands with a Trimethylbenzene Core. *J. Mex. Chem. Soc.* **2011**, *55*, 168–175.

(43) Minato, I.; Shibata, K.; Fujinami, K. *Polyglycidyl Compounds*. U.S. Patent US 4,400,525 A, 1983.

(44) Forse, A. C.; Milner, P. J.; Lee, J. H.; Redfearn, H. N.; Oktawiec, J.; Siegelman, R. L.; Martell, J. D.; Dinakar, B.; Zasada, L. B.; Gonzalez, M. I.; Neaton, J. B.; Long, J. R.; Reimer, J. A. Elucidating CO₂ Chemisorption in Diamine-Appended Metal–Organic Frameworks. *J. Am. Chem. Soc.* **2018**, *140*, 18016–18031.

(45) Noble, J. A.; Theule, P.; Duvernay, F.; Danger, G.; Chiavassa, T.; Ghesquiere, P.; Minevac, T.; Talbi, D. Kinetics of the NH₃ and CO₂ Solid-State Reaction at Low Temperature. *Phys. Chem. Chem. Phys.* **2014**, *16*, 23604–23615.

(46) Lim, T. H.; Foster, J. E.; Ellis, B. R.; Skerlos, S. J. Microwave-Based CO₂ Desorption for Enhanced Direct Air Capture: Experimental Validation and Techno-Economic Perspectives. *Environ. Res. Lett.* **2024**, *19*, No. 034002.